RSC Advances

ROYAL SOCIETY OF CHEMISTRY

www.rsc.org/advances

Structure variations of series lanthanide complexes constructed from quinoline carboxylate ligand: photoluminescent properties and PMMA matrices doping

Huijie Zhang,[a] Ruiqing Fan,*[,a] Ping Wang,[a] Xinming Wang,[a] Song Gao,[a] Yuwei Dong,[a] Yulei Wang,[b] Yulin Yang*[,a]

[a]Department of Chemistry, Harbin Institute of Technology, Harbin 150001, P. R. of China

[b]National Key Laboratory of Science and Technology on Tunable Laser, Harbin Institute of Technology, Harbin 150080, P. R. of China

To whom the proofs and correspondence should be sent.

Professor Rui–Qing Fan and Yu–Lin Yang
Department of Chemistry
Harbin Institute of Technology Harbin 150001, P. R. China
Fax: +86–451–86413710
E–mail: fanruiqing@hit.edu.cn and ylyang@hit.edu.cn

Series lanthanide complexes formulated as $\{[KEu(Hqlc)(qlc)(H_2O)_6(OH)]^{2+}\cdot 2Cl^-\}_n$ (**1·Eu**), $\{[Eu(qlc)_2(phen)(H_2O)_2]^+\cdot Cl^-\}\cdot CH_3CN$ (**2·Eu**), $[Eu(qlc)_2(phen)(NO_3)]\cdot H_2O$ (**3·Eu**), $[Ln(qlc)_2(H_2O)_4]\cdot(qlc)\cdot(H_2O)$ (Ln = Eu(**4·Eu**), Sm(**5·Sm**), Gd(**6·Gd**), Tb(**7·Tb**), Dy(**8·Dy**), Ho(**9·Ho**)) (Hqlc = quinoline–3–carboxylic acid, phen = 1,10–phenanthrolin) synthesized under solvo(hydro)thermal conditions and characterized by single–crystal X–ray diffraction, infrared spectra, elemental analysis, and powder X–ray diffraction. Complex **1** exhibits two–dimensional (6,3)-connected *hcb* networks and possesses stable structure through typical O/C–H···Cl intermolecular hydrogen bonds. Complexes **2–4** display three diverse dimer structures, due to the synergistic effect from coordination modes of Hqlc ligand and anion effect. Complexes **5-9** are isostructural with complex **4**. Eu–complexes **1–4** could be triggered intense and bright characteristic $^5D_0\rightarrow{}^7F_J$ red luminescence under UV excitation in the solid state at 298 K and 77 K. In complexes **2** and **3**, coordinate phen ligand could play the antenna role in the energy transfer process. Therefore, the luminescence lifetimes of complexes **2** (779.62 and 792.65μs) and **3** (947.21 and 1095.59 μs) are longer than those of complexes **1** (456.93 and 499.33 μs) and **4** (283.70 and 46469 μs) in the solid state at 298 K and 77 K. Complexes **5**, **7** and **8** exhibit characteristic Sm^{3+}, Tb^{3+} and Dy^{3+} ions luminescence. Furthermore, through controlling concentration of complexes **3** and **4** in poly(methyl mathacrylate) (PMMA), a series of **3**–PMMA and **4**–PMMA hybrid materials are obtained, respectively. They all display strong and characteristic red luminescence emissions at concentration of 8%. Compared with **3** and **4**, the luminesence intensities and luninescence lifetimes of **3-**PMMA and **4–**PMMA are increased, due to the replacement of water molecules by PMMA.

Introduction

Taking advantage of the versatile photophysical properties of Ln^{3+} ion, its sharp, intense, and recognizable *f*→*f* transitions that are almost independent of the nature of the chemical environment and their excited–state lifetimes, which are usually long enough to allow time–resolved detection. Now, luminescent lanthanide materials have received increasing attention for applications in the field of smart and hybrid materials.[1–4] Whereas, lanthanide ions usually suffer from weak light absorption due to the forbidden *f*→*f* transitions (Laporte fobidden), leading to inefficient and inappropriate of the direct excitation of metal ions.[5,6] Through an "antenna effect", sensitization of the Ln^{3+} ions with the organic antenna molecule can be achieved by a ligand–to–metal energy–transfer.[7–9] To be effective, it is necessary for the energy levels of the donor to be near enough for the acceptor to allow energy transfer occur. Furthermore, the energy levels of donor is not located too close resulting loss of energy via back–transfer to be donor or other energy migration pathways.[10] Among the present sensitizers, several quinoline–based chromophores attract noble attention for constructing luminescent complexes; for example, tri–8–(hydroxyquinoline) aluminum has been developed as an efficient electroluminescence material in organic light emitting diode (OLED) fabrication.[11] Besides, various non–covalent weak interactions such as π–π stacking interactions and hydrogen bonding play significant roles to stabilize the supramolecular networks.[12–14] Considered about the disadvantage of poor mechanical property for Eu^{3+} complexes, they were usually applied as the organic–inorganic hybrid materials through physical doping or grafting into stable organic or inorganic matrices.[15–18] Therefore, when Eu^{3+} complexes are doped into PMMA to form polymer films, improved flexibility, versatility, and photo–stability properties of luminescent materials could be expected.

Taking account of the above, we prepared a novel series lanthanide complexes $\{[KEu(Hqlc)(qlc)(H_2O)_6(OH)]^{2+}\cdot 2Cl^-\}_n$ (**1·Eu**), $\{[Eu(qlc)_2(phen)(H_2O)_2]^+\cdot Cl^-\}\cdot CH_3CN$ (**2·Eu**), $[Eu(qlc)_2(phen)(NO_3)]\cdot H_2O$ (**3·Eu**), $[Ln(qlc)_2(H_2O)_4]\cdot(qlc)\cdot(H_2O)$ (Ln = Eu(**4·Eu**), Sm(**5·Sm**), Gd(**6·Gd**), Tb(**7·Tb**), Dy(**8·Dy**), Ho(**9·Ho**)) under solvo(hydro)thermal conditions. Quinoline–3–carboxylic acid which comes from quinoline–2,3–carboxylic acid under *in–situ* decarboxylation was studied as candidate.[19] The structure diversities are mainly depending on the coordination modes of Hqlc ligand and counterions. The neutral phen ligand plays the

antenna role participated in the energy transfer process, which enhances the luminescence intensities and luminescence lifetimes of **2** and **3**. The photoluminescence properties of **3**–PMMA and **4**–PMMA were discussed in details.

Results and discussion

Synthesis and characterization

The reaction routes of **1–4** are shown in Scheme 1. Solvo(hydro)thermal methods[20–22] were employed in this work for the syntheses of the complexes. In our work, *in–situ* decarboxylation occurred at quinoline–2,3–dicarboxylic acid (H_2qldc) when it reacted with lanthanide salts. The ligand 2,3–H_2qldc easily lost one 2–position carboxyl group under high temperature (120 °C–160 °C) and produced quinoline–3–carboxylic acid (Hqlc), as shown in Scheme S1. This result is confirmed by ^{13}C NMR analysis. As shown in Fig. S1, the characteristic peaks of –COOH appeared at 167.99 and 166.22 ppm for H_2qldc, and the reaction product displayed one characteristic peak of –COOH at 166.30 ppm.

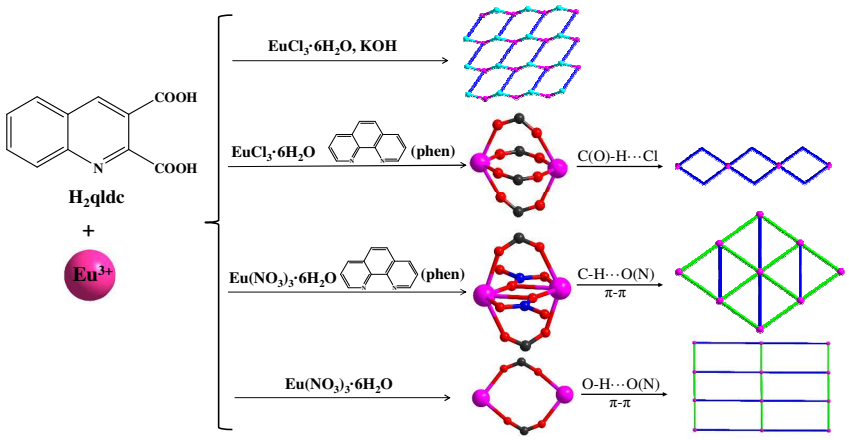

Scheme 1. The reaction routes of complexes **1–4**.

In the structure of **1**, K^+ ions acts as structure–directing agents incorporated into the resulting crystalline materials. When chelate ligand phen was introduced during the assembly of lanthanide complexes to increase the rigidity of the system, dimer complexes **2** and **3** were obtained with different counterions (Cl^- and NO_3^-). Complexes **4–9** are isostructure which are connected by two III–qlc^- ligands. Scheme S2 summarizes the coordination modes of qlc^- ligand in the nine complexes. The Cl^- ion flexibly coordinates with metal ions or frees in crystal structure to balance the charge (complexes **1** and **2**). The Cl^- ion is also involving in the construction

supramolecules with a typcial intermolecular hydrogen bonding (O/C–H···Cl).[23] As for the nitrate anion, it often inclines to strongly chelate to metal ions, acting as a terminal ligand (complex **3** and **4**).[24] Based on the above analysis, the formation of final complexes are the synergistic effect from coordination modes and anion effect.

Complexes **1–9** possess the same coordinated qlc^- ligand and the IR spectra are similar. The strong and broad absorption bands in the range of 3000–3500 cm^{-1} in complexes **1–9** are assigned as characteristic peaks of O–H vibration. The strong vibrations appearing around 1600 and 1400 cm^{-1} correspond to the asymmetric and symmetric stretching vibrations of the carboxylate group, respectively. The absence of strong absorption bands at ca. 1700 cm^{-1} indicates H_2qldc ligand is completely deprotonated, as shown in Fig. S2 and S3. The O–C–O vibration in plane occurs in middle intensity peaks in the range of 580–800 cm^{-1}. Moreover, the weak absorption bands in IR spectra of **2** and **3** at 464 and 474 cm^{-1} are assigned to the stretching vibration of Eu–N bond.[25]

Crystal structures

$\{[KEu(Hqlc)(qlc)_2(H_2O)_6(OH)]^{2+}\cdot 2Cl^-\}_n$ (1). Single–crystal X–ray diffraction analysis reveals that complex **1** crystalizes in the monoclinic *P*c space group, which exhibits 2D (6,3)-connected *hcb* network. The asymmetric unit of **1** consists of one crystallographically unique Eu^{3+} cation, one K^+ cation, one fully–deprotonated qlc^- anion, one Hqlc ligand, six coordinated water molecules, one OH^- anion, and two free Cl^- anions. Each central Eu^{3+} ion is nine–coordinated by two oxygen atoms (O1 and O4) from two different Hqlc ligands, seven oxygen atoms from six water molecules and OH^- anion resulting in the tricapped trigonal prism geometry, as illustrated in Fig. S4. The Eu–O distances vary from 2.282(17) to 2.603(11) Å. Each K^+ ion is four–coordinated by three oxygen atoms from three different water molecules and one nitrogen atom (N1) from II-Hqlc ligand. Thus, the four–coordinated K^+ atom forms a tetrahedron. The K–O distances are 3.049(16), 3.060(15), and 3.202(19) Å, respectively, and K-N distance is 3.030(20) Å, which are in accordance with reported values in other europium–potassium complexes.[26] Adjacent two Eu^{3+} ions linked two I-qlc^- ligand at both sides that are bridge by potassium and water molecules to form an infinite 1D chain structure (Fig. 1a). The 1D chains are further bridged through N1 atom from II-Hqlc ligand forming a 2D layer structure (Fig. 1b). If ignoring the K^+ ion, complex **1** is only a discrete structure. Therefore, the K^+ ion directs and changes

the structure formation of **1**. Furthermore, the H···Cl distances between the OH and chlorine atoms from neighboring chains are shorter than the sum of van der Waals radii for H and Cl (ca. 1.2 Å for H, 1.75 Å for Cl), and the angle are in the range of 131.22–163.93 °, which indicate the typcial intermolecular hydrogen bonds existence in the structure of **1**, as shown in Fig. 1c. If we ignoring I-qlc$^-$ ligand, the metal centers (Eu and K atoms) are viewed as the nodes and the Hqlc ligands as linkers, the resulted 2D structure may be simplifed into a (6,3)-connected *hcb* network as depicted in Fig. 1d.

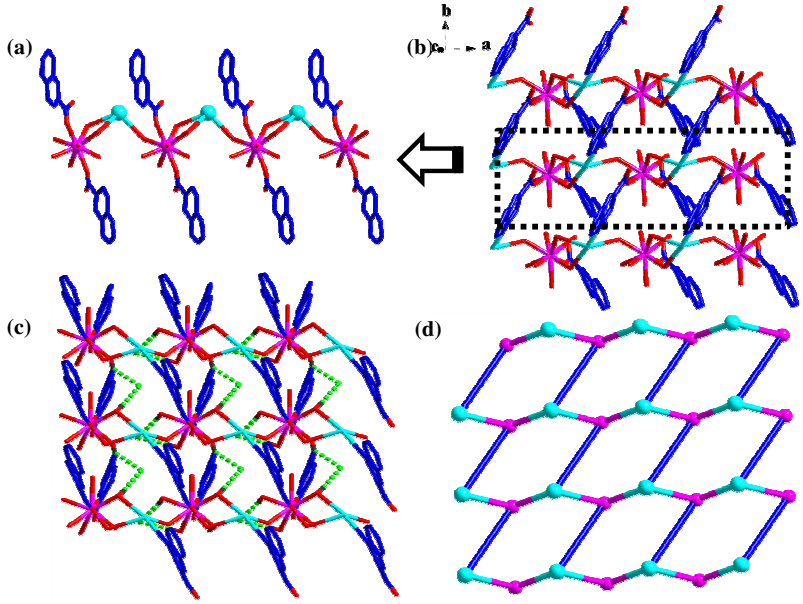

Fig. 1 (a) Ball-and-stick representation of the 1D chain structure. (b) The 2D layer structure of **1**. (c) View of the intermolecular hydrogen bonding O–H···Cl in complex **1** (hydrogen bonding are shown by green dashed line). (d) The 2D (6,3)-connected *hcb* topology in its symmetrical form distinguished by different colors (Eu^{3+}, pink ball; K^+, light blue ball; Hqlc, deep blue linkers).

{[Eu(qlc)$_2$(phen)(H$_2$O)$_2$]$^+$·Cl$^-$}·CH$_3$CN (2). Single–crystal X–ray diffraction analysis reveals that complex **2** crystalizes in the triclinic $P\bar{1}$ space group, which features a dimer structure connected by Hqlc ligand. The asymmetric unit of **2** consists of one crystallographically unique Eu^{3+} cation, two fully–deprotonated qlc$^-$ anions, one phen, two coordinated water molecules, one free CH_3CN and free Cl^- anion, as shown in Fig. 2a. Each central Eu^{3+} ion is eight–coordinated by four oxygen atoms (O1, O2A, O3, and O4) from four qlc$^-$ ligands, two oxygen atoms (O5 and O6) from two H_2O, and two nitrogen atoms (N1 and N2) from phen ligand, resulting in the bicapped trigonal prism geometry (Fig. S5). The distances between the two coordinated nitrogen atoms with Eu^{3+} are 2.594 (8) Å (Eu1–N1) and 2.647 (8) Å (Eu1–N2),

respectively. The Eu–O distances vary from 2.319 (3) to 2.480 (3) Å in accordance with reported values in other europium complexes.[27] The average bond length of the Eu–$O_{carboxyl}$ is 2.341 Å, which is slightly shorter than that of Eu–O_{water} (2.452 Å). It is attributed to that of Eu–$O_{carboxyl}$ is stronger than the covalent bond of Eu–O_{water}. Eu1 and its corresponding centrosymmetric generated atom Eu1A (symmetry code A = 2–x, 2–y, 1–z) are joined by two bidentate bridged carboxylic groups (III-qlc$^-$) to form a binuclear unit, with the separation of Eu···Eu being 4.364 Å, as shown in Fig. 2b. The cationic charge $[Eu(qlc)_2(phen)(H_2O)_2]^+$ moieties is balanced by the one free Cl^- anion, which can serve as the acceptor of hydrogen bond. The 1D chain structure is obtained by intermolecular hydrogen bonding interactions which are formed by uncoordinated Cl^- anion and coordinated water molecules (O5 and O6). Furthermore, the C25–H25···Cl1 hydrogen bonding interaction is involing in the structure stability (Fig. 2c). If considering the dimer structure as nodes and these hydrogen bonds (O–H···Cl and C–H···Cl) as 'V'-shaped linker, a beaded chain of **2** is created (Fig. 2d).

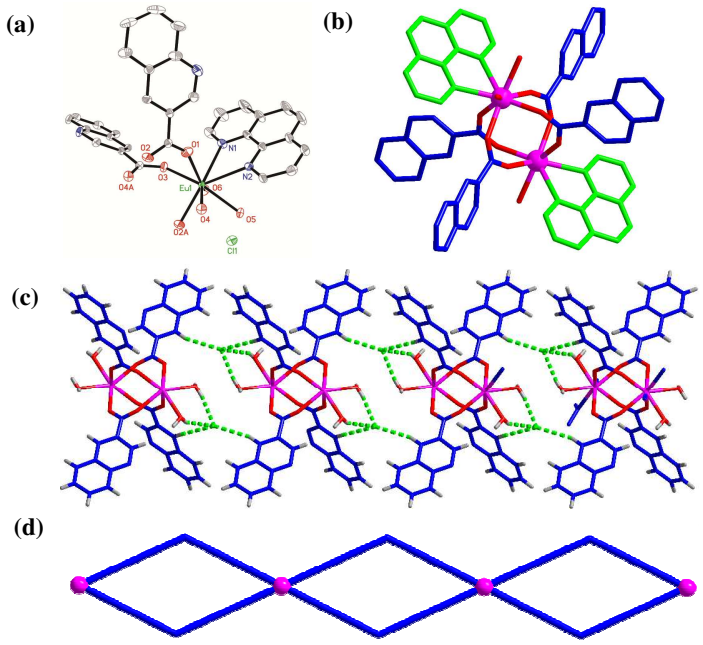

Fig. 2 (a) The metal coordination environment in **2** with labeling scheme and 50% thermal ellipsoids (hydrogen atoms and free CH_3CN are omitted for clarity). (b) Ball-and-stick representation the dimer structure of complex **2**. (c) 1D supramolecular structure of **2** (hydrogen bonding are shown by green dashed line). (d) The beaded chain structure of complex **2**.

$[Eu(qlc)_2(phen)(NO_3)]\cdot H_2O$ (3). Single–crystal X–ray diffraction analysis reveals that complex **3** crystalizes in the monoclinic $P2_1/n$ space group, which features a

dimer structure connected by NO_3^- and qlc$^-$ ligand. As shown Fig. S6, the asymmetric unit of **3** consists of one crystallographically unique Eu^{3+} cation, two fully–deprotonated qlc$^-$ anion, one phen ligand, one nitrate anion, and one free water molecular. Each Eu^{3+} center is nine–coordinated with seven oxygen atoms, including four carboxylic oxygen atoms (O1, O2A, O3, and O4) from three qlc$^-$ ligands, and three oxygen atoms (O5, O5A, and O6) from two NO_3^- anions. The uncoordinated sites are occupied by two nitrogen atoms (N3 and N4) from phen ligand. As a result, the coordination geometry around the metal center can be best described as distorted tricapped trigonal prism geometry. Eu1 and its corresponding centrosymmetric generated atom Eu1A (symmetry code A = 1–x, 2–y, –z) are joined by two bidentate bridged carboxylic groups (III-qlc$^-$) and NO_3^- anions to form a binuclear unit, with the separation of Eu···Eu being 3.943 Å (Fig. 3a). This distance is shortest among complexes **2–4**, because of the NO_3^- anions connected the adjacent metal centers, which narrowing the distance of two metal centers. It is worth noting that π···π interactions and hydrogen bonding play critical roles to stabilize the structure.[28] The pyridyl ring of qlc$^-$ ligand and phen plane take place in a face-to face mode, with the intercentroid distances 3.589 Å (Fig. 3b). The moieties are extended to into a 2D supramolecular framework through the C–H···N and C–H···O hydrogen bonding interactions (C22–H22A···N2 = 2.661 Å and C25–H25A···O6 = 2.608 Å), as displayed in Fig. 3c. If the dimer structure is viewed as the node and hydrogen bonds or π···π stacking interactions as linkers, the resulted 2D supramolecular structure may be simplified into a "dense" (3,6) network, as shown in Fig. 3d.

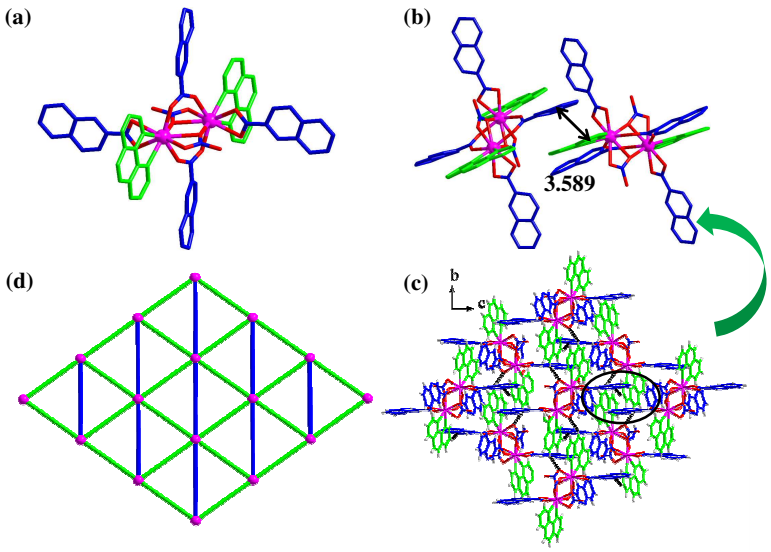

Fig. 3 (a) Ball-and-stick representation the dimer structure of complex **3**. (b) The π-π interactions between the two face-to-face pyridyl ring and benzene ring (c) A 2D supramolecular structure of complex **3** constructed by hydrogen bonds and π···π stacking interactions along a axis. (d) View of the 2D supramolecular layer (3,6) network in complex **3**.

$[Ln(qlc)_2(H_2O)_4]\cdot(qlc)\cdot(H_2O)$ (Ln = Eu(4), Sm(5), Gd(6), Tb(7), Dy(8), Ho(9)). Single–crystal X–ray diffraction analysis reveals that complexes **4–9** are isomorpous and crystallizes in the triclinic $P\bar{1}$ space group, which feature dimer structure. Only the structure of **4** is described in detail. The asymmetric unit of **4** consists of one independent Eu^{3+} cation, two fully–deprotonated qlc^- anion, four coordinated water molecules, one free fully–deprotonated qlc^- anion and one free water molecule with all in general positions. The Eu^{3+} center is eight coordinated, with four oxygen atoms (O1A, O2, O3, and O4) derived from two qlc^- ligands and four oxygen atoms (O7, O8, O9, and O10) derived from four terminal coordinated water molecules, forming a distorted bicapped trigonal prism geometry, as displayed in Fig. S7. The bond lengths of Eu–O vary from 2.303 (7) to 2.453 (8) Å. O–Eu–O band angles are in the range of 53.2 (3) °–154.0 (3) °. All the Eu–O distances and O–Eu–O bond angles are closed to the values found in other Eu^{3+} complexes.[29] The average bond length of Ln–O(carboxyl) decreases with decreasing the radii of the Ln ions.[30] Two equivalent Eu^{3+} centers are bridged by III–qlc^- ligand to give a dimer lanthanide structure with separations of Eu···Eu (5.320 Å), as shown in Fig. 4a. The Eu···Eu distance is the longest among the four complexes. Because the adjacent metal centers are connected through two III-qlc^- ligands, the carboxylic acid group could stretch better. In complex **4**, following ones can be found: O–H···O, O–H···N, donor···acceptor distance is in the range of 2.723–3.354 Å. The shortest distance 2.723 Å refers to the intramolecular O7–H4C···O6 (∠OHO = 117.73°) hydrogen bond. The intermolecular hydrogen bonding connected the dimer structure into 1D chains (Fig. 4b). The 1D chains are further assembled into 2D supramolecular layer structure through inter-layer π–π stacking interactions between the adjacent quinolone rings, as shown in Fig. 4c. The π–π stacking distance between two benzene rings is 3.351 Å. The two quinoline–ring planes are nearly parallel geometry with the dihedral angle is 1.017 °. Similar to complexes **2** and **3**, through these weak interactions a 2D supramolecular network is constructed, as shown in Fig. 4d, in which each dimer links four adjacent ones. Thus, the overall topology of **4** can be defined as 4^4 topology. The hydrogen bonding interactions in complexes **1–9** are listed in Table S3.

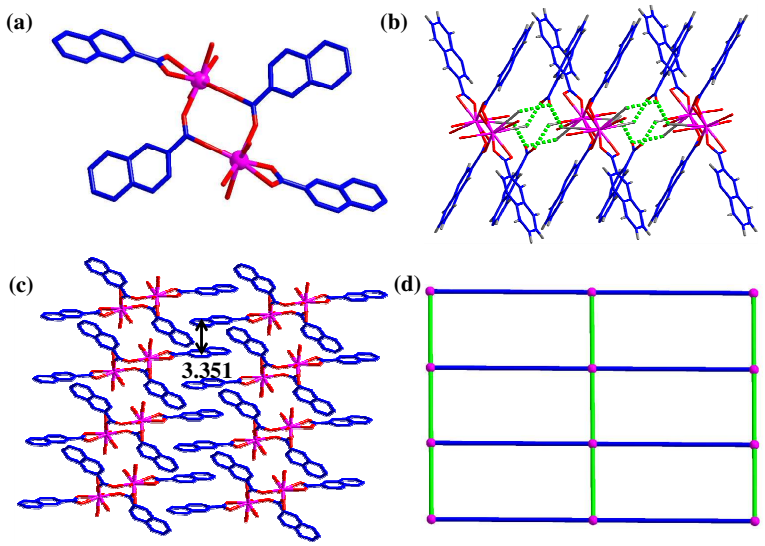

Fig. 4 (a) Ball-and-stick representation the dimer structure of **4**. (b) A 1D supramolecular structure constructed by intermolecular hydrogen bonding O–H···O and O–H···N in complex **4**. (c) A 2D supramolecular network constructed by π-π stacking interactions between the two face-to-face pyridyl rings. (d) View of the 2D supramolecular layer structure with 4^4 topology.

Powder X–ray diffraction (PXRD) has been used to check the phase purity of the bulky samples in the solid state. As shown in Fig. S8, the experiment PXRD patterns of **1–9** are in good agreement with those simulated from their single–crystal X–ray data, indicating the purity of the as–synthesized products. The differences in intensities may be due to the preferred orientation of the powder samples.

Photoluminescence (PL) Properties

The luminescent properties of ligand and complexes **1-8** were examined in the solid state at 298 K or 77 K and summarized in Table S4, Figures 5-7 and Fig. S10-S12. Upon excitation at from 320 to 365 nm, which are the maximum of the excitation spectra, complexes **1–4** show the characteristic narrow emission bands of the Eu^{3+} ion corresponding to the $^5D_0 \rightarrow {}^7F_J$ (J = 0–4) transitions, as illustrated in Fig. 5. Among them, the $^5D_0 \rightarrow {}^7F_2$ transition at λ = 613 nm is the strongest emission that is an induced electric dipole transition, and its corresponding intensity is very sensitive to the coordination environment. The very intense $^5D_0 \rightarrow {}^7F_2$ peak, pointing to a highly polarizable chemical environment around the Eu^{3+} ion and is responsible for the brilliant red emission of complexes **1–4**. Furthermore, the emission spectra of complexes **1–4** show only one peak for the $^5D_0 \rightarrow {}^7F_0$ transition and three stark components for the $^5D_0 \rightarrow {}^7F_1$ transition, indicating the presence of a single chemical environment around the Eu^{3+} ion. The emission bands around 578 and 650 nm are very weak, since their corresponding transitions $^5D_0 \rightarrow {}^7F_{0,3}$ are forbidden both in

magnetic and electric dipole schemes. The emission band at 699 nm is attributed to $^5D_0 \rightarrow {}^7F_4$ transition. The absence of bands from higher excited states such as $^5D_1$ in the emission spectrum implies that the nonradiative relaxation to the $^5D_0$ level is efficient.[31] Additionally, the luminescent intensities of **1–4** in the solid state at 77 K are higher than those at 298 K, due to the O–H oscillators are protected at low temperature.[5]

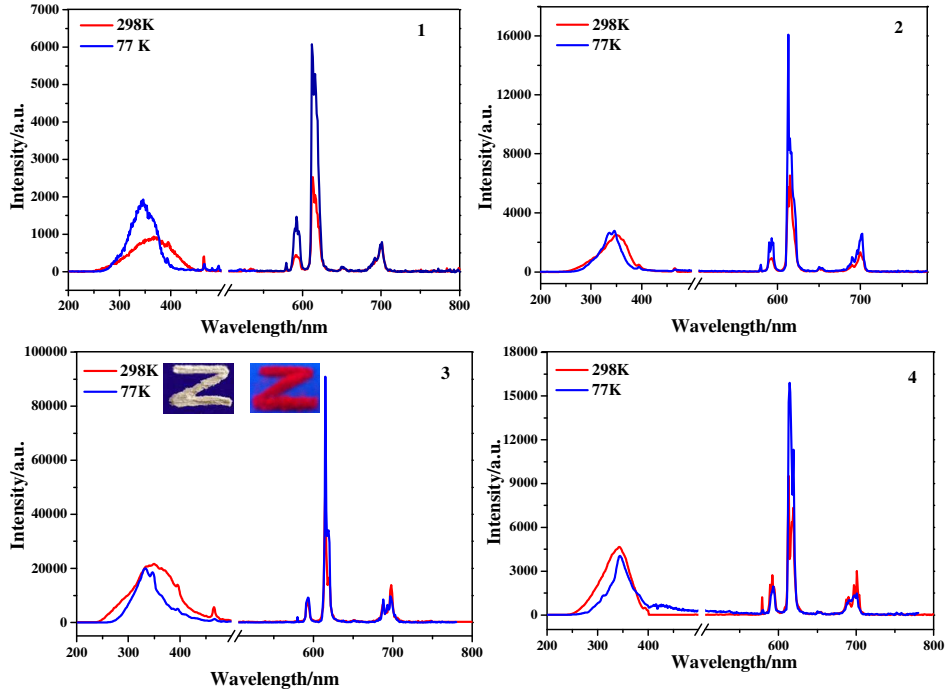

Fig. 5 Solid-state excitation and emission spectra of complexes **1–4** both at 298 K and 77 K (The inset shows the photographs of complex **3** under UV lamp).

The decay curves of **1–4** were measured at both 298 K and 77 K and monitored within the most intense lines of the $^5D_0 \rightarrow {}^7F_2$ transition. The observed luminescent decay profiles correspond to single exponential functions at 298 K and 77 K. The luminescence lifetimes in the solid state are determine to be 456.93, 779.62, 947.21, and 283.70 μs at 298 K. At 77 K, the τ values (499.33 for **1**, 792.65 for **2**, 1098.59 for **3**, and 464.69 μs for **4**) are much higher than those at 298 K to 77 K, due to the absence of thermally activated deactivation processes. These complexes show increasing luminescence lifetime as sequence **4** < **1** < **2** < **3** both at 298 K and 77 K. The shortest $^5D_0$ lifetime noted for the Eu^{3+} complex **4** maybe due to the dominant nonradiative decay channels associated with vibronic coupling because of the presence of four coordinate water molecules. As a result of the potassium-to-europium charge transfer (MMCT) [32] in **1**, the luminescence lifetime of

1 is longer than **4**, though there are more water molecules in **1**. The photoluminescence is closely related to the local environments around metal ions, as the Eu···Eu distances and Eu–N bond lengths are shortest in complex **3**, the energy levels are lowered. Therefore, the luminescence lifetime of **3** is the longest.

As shown in Fig 6, the excitation spectra of complex **7**, which monitored the intense characteristic emission (545 nm) of the Tb^{3+} ion, displays broad band with peak at 360 (298 K) and 330 nm (77 K) for the electronic transitions of Hqlc ligand. The emission spectrum of **7** shows characteristic Tb^{3+} metal–centered and ligand–centered luminescence, respectively. The ligand–centered emission (412 nm at 298 K and 423 nm at 77 K) is red–shifted compared with free ligand (400 nm), which may be attributed to the metal–disturbed ligand–centered $\pi^*\rightarrow\pi$ transitions.[33] Complex **7** shows four line–like emission bands at 490, 545, 584, and 621 nm, which results from deactivation of the $^5D_4$ excited state to the corresponding ground states ^7F_J (J = 6, 5, 4, 3) of Tb^{3+} ion. The $^5D_4\rightarrow{}^7F_5$ transition at 545 nm is the strongest emission, implying intense green luminescence. Besides, the transitions to ^7F_J (J = 2, 1, 0) levels are too weak to measure.[34] The luminescence lifetime of complex **7** at 77 K (8.77 μs) is longer than it at 298 K (5.55 μs).

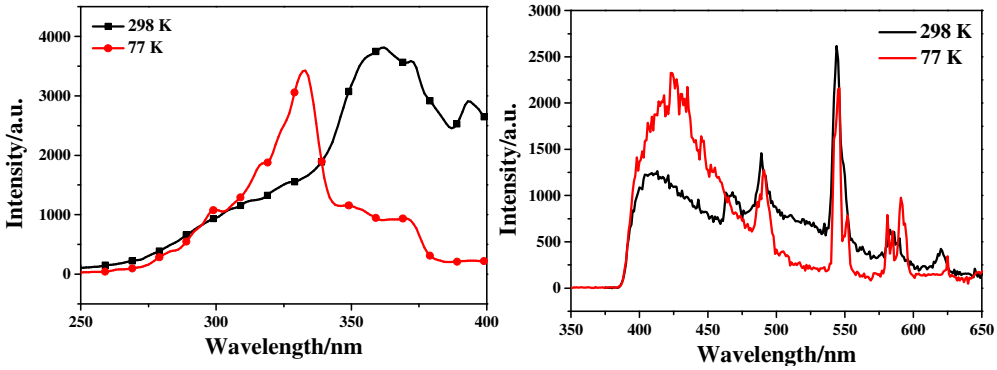

Fig. 6 Excitation and emission spectra of complex **7** in the solid state at 298 K and 77 K

The solid state visible luminescence of complexes **5** and **8** were investigated at room temperature and liquid nitrogen temperature (Fig. 7). Upon excitation at 325 nm, which is the maximum of the excitation spectrum, complex **5** shows characteristic narrow band emissions of Sm^{3+} ion corresponding to the $^4G_{5/2}\rightarrow{}^6H_{5/2}$ (562 nm), $^4G_{5/2}\rightarrow{}^6H_{7/2}$ (596 nm), $^4G_{5/2}\rightarrow{}^6H_{9/2}$ (644 nm), and $^4G_{5/2}\rightarrow{}^6H_{11/2}$ (700 nm), as shown in Fig. 8. The ligand–centered emission (430 nm at 298 K and 415 at 77 K) is red–shifted compared with free ligand, which may be attributed to the metal disturbed ligand–centered $\pi^*\rightarrow\pi$ transitions.[33] The lifetimes of $^4G_{5/2}$ amounts to 21.43 μs at 298

K and 21.77 μs at 77 K. Upon excitation at 325 nm, complex **8** shows characteristic narrow band emissions of Dy^{3+} ion corresponding to $^4F_{9/2}\rightarrow{}^6H_{15/2}$ (481 nm), $^4F_{9/2}\rightarrow{}^6H_{13/2}$ (574 nm), $^4F_{9/2}\rightarrow{}^6H_{11/2}$ (661 nm), and $^4F_{9/2}\rightarrow{}^6H_{9/2}+{}^6F_{11/2}$ (750 nm). The characteristic $^4F_{9/2}\rightarrow{}^6H_{9/2}+{}^6F_{11/2}$ transition is rarely observed and described.[35] We have observed ligand–centered π*→π transitions (420 nm at 298 K and 405 nm at 77 K). The lifetimes of $^4F_{9/2}$ amounts to 7.09 μs at 298 K and 7.97 μs at 77 K.

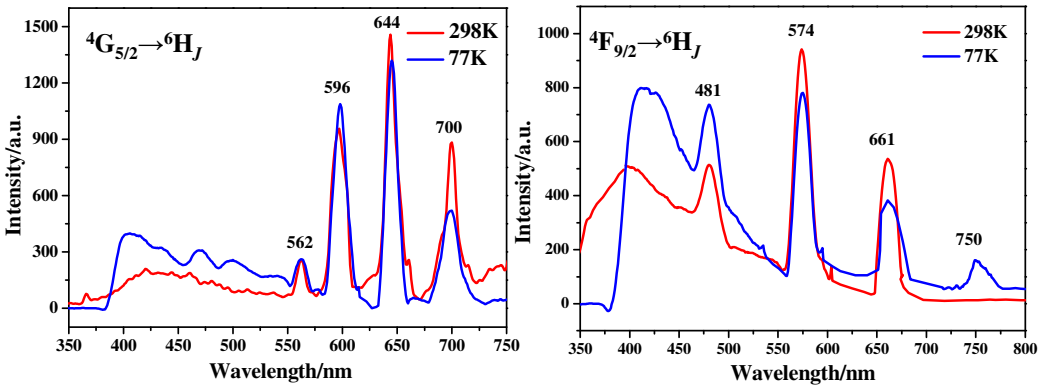

Fig. 7 Emission spectra of complexes **5** (left) and **8** (right) in the solid state at 298 K and 77 K.

We have also observed emissions in the near infrared region from the Sm^{3+} and Dy^{3+} ions (Fig. S11), which is a rarely described phenomenon.[36,37] The emission spectrum of **5** consists of several bands at λ = 936, 988, 1193, 1285, and 1383 nm are clearly observed. Emission peaks at 936 nm, 988 nm and 1193 nm and 1196 nm are suspected to be the Stark splitting of $^6F_{5/2}$, $^6F_{7/2}$ and $^6F_{9/2}$, respectively. The other emissions are assigned to the *f*–*f* transitions of $^6F_{11/2}$ (1285 nm and 1383 nm), respectively. The emission bands of **5** are shifted relative to the bands of the reported theoretical values. The emission spectrum of **8** consists of several bands at λ = 948, 985, and 1187 nm, which are attributed to the *f*–*f* transitions $^4F_{9/2}\rightarrow{}^6F_{7/2}$, $^4F_{9/2}\rightarrow{}^6F_{5/2}$, and $^4F_{9/2}\rightarrow{}^6F_{3/2}$, respectively.

Energy Transfer Process

The data of the triplet excited state T_1 of ligand (23809 cm^{-1}) was calculated by the low–temperature (77 K) phosphorescence spectrum of the complex **6**. The singlet energy level (S_1) of Hqlc ligand is 28169 cm^{-1} (355 nm), which is calculated from the UV–Vis absorbance edges (Fig. S12). The singlet and triplet energy levels of phen (31000 and 22100 cm^{-1}) were taken from the literature.[38] In a typical example of complex **3**, the energy transfer process is discussed. As it is known that the intersystem crossing process becomes effective when ΔE ($^1\pi\pi^*-{}^3\pi\pi^*$) is at least 5000 cm^{-1}, the energy gap ΔE ($^1\pi\pi^*-{}^3\pi\pi^*$) for Hqlc ligand and phen are 4369 cm^{-1} and

8900 cm^{-1}, respectively. It indicates that the intersystem crossing is effective in phen ligand.[39] Otherwise, the energy gap between $^3\pi\pi^*$ (qlc^- ligand) and $^1\pi\pi^*$ (phen ligand) is 6069 cm^{-1}. It indicates that the energy may transfer from qlc^- to phen ligand. The energy difference between the lowest triplet state of phen and the resonant energy levels of Eu^{3+} ($^5D_1$, 18674 cm^{-1}) is 3426 cm^{-1}. According to the empirical rule proposed by Latva,[40] for an optimal ligand–to–metal energy transfer process for Eu^{3+} needs 2500–4500 cm^{-1}, the energy differences in Scheme 2 therefore show that the transitions is effective from the triplet energy level of phen to Eu^{3+} ion. The absence of bands from higher excited states such as $^5D_1$ in the emission spectrum implies that the nonradiative relaxation to the $^5D_0$ level is efficient. According to the consideration of the above, the emission intensity and luminescence lifetime of complexes **2** and **3** are enhanced because of the ligand to metal energy transfer processes could occur in the mixed ligand complexes.

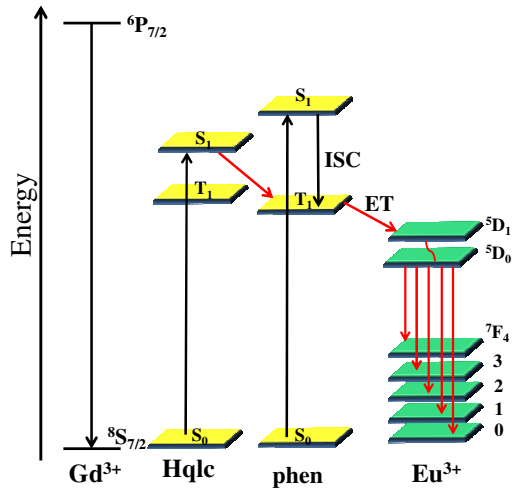

Scheme 2 Schematic energy level diagram and energy transfer process.

Properties of complexes 3 and 4 doped into PMMA polymer films

In consideration of the excellent performance of PMMA as one of the most popular polymer matrices with low cost, easily prepared, and good mechanical property,[41,42] two PMMA-supported hybrid materials **3**-PMMA and **4**-PMMA are obtained from complexes **3** and **4**, respectively. The excitation and emission spectra of PMMA polymer doped with complexes **3** and **4** at different concentrations (2%, 4%, 6%, 8%, and 10%) are shown in Fig. 8. The excitation spectra are dominated by intense broad bands at 325 nm and 330 nm, which can be assigned to absorptions of both the PMMA polymer and the organic chromophore. The emission spectra **3**-PMMA and

4-PMMA at a variety of concentrations exhibit five emission bands that are assigned to the characteristic $^5D_0 \rightarrow {}^7F_J$ (J = 0–4) transitions of Eu^{3+} ion. The luminescent intensity of Eu^{3+} emission at 613 nm is strengthened with the concentration of complexes **3** and **4** increased and reaches a maximum at concentration of 8%. Further increases in the concentration lead to a decrease the luminescent intensity. The energy transfer between the lanthanide ions themselves is a nonradiative process, which accounts for the decrease in the Eu^{3+} emission, especially at high concentration (10%).[43] The luminescence decay curves of the doped films were obtained by monitoring the emission at the hypersensitive $^5D_0 \rightarrow {}^7F_2$ (613 nm). These data were adjusted with mono–exponential decay function and the lifetime values (τ) of the emitter $^5D_0$ level of the doped systems were determined and are listed in Table S5. As shown in Fig. S13, the luminescence lifetimes for **3**–PMMA and **4**–PMMA are higher than complexes **3** and **4**, thus indicating that radiative process are operative in the doped polymer films because of the absence of O–H oscillators from the water molecules. Compared the emission spectra of **3, 4, 3**–PMMA and **4**–PMMA, the luminescence intensities are in the sequence of **3**–PMMA > **3** > **4**–PMMA > **4**. The reason of the emission intensity of **3** > **4** is caused by the substitution of the water molecules by the bidentate nitrogen donors in complex **3**. Luninescent lifetime of **4**–PMMA (τ = 972.33 μs) increases nearly three times longer than complex **4** (τ = 283.70 μs) and luminescent intensity is twice of **4** (Fig. S14), due to structure of **4** has more coordinate water molecules than **3**.

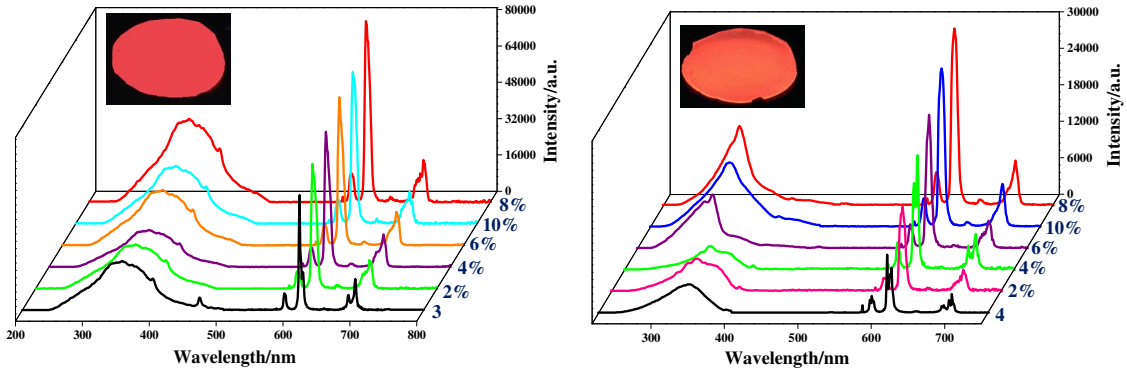

(a) (b)

Fig. 8 Excitation and emission spectra of **3**–PMMA and **4**–PMMA films doped with 2 to 10% of **3** and **4**.

Conclusion

In summary, series of lanthanide complexes have been synthesized with H_2qldc under

solvo(hydro)thermal conditions. The K^+ ion acts as structure–directing agent and connected adjacent Eu^{3+} ion through water molecules and nitrogen atom from Hqlc ligand to form a 2D (6,3)-connected *hcb* network in **1**. Complexes **2–4** display three diverse dimer structures due to the different coordination modes and anion effect. These complexes show increasing luminescence lifetimes as sequence **4 < 1 < 2 < 3** both at 298 K and 77 K, which are closely related to their structure models. The photoluminescence properties study on complexes **1–4** demonstrate that the Eu^{3+} luminescence is well–sensitized by Hqlc and phen ligands, indicating efficient energy transfer process from ligands to Eu^{3+} ions in complexes **2** and **3**. Moreover, PMMA enhances the luminescent intensity and luminescent lifetimes of the PMMA film doped with complexes **3** and **4** in comparison with the precursor complexes. Therefore, the PMMA doped with the luminescent lanthanide complexes may be of potential applications as light–emitting materials and active polymer optical devices.

Supplementary Materials

No. 1041890-1041898 contains the supplementary crystallographic data for complexes **1–9**. These data can be obtained free of charge via http://www.ccdc.cam.ac.uk/conts/retrieving.html, or from the Cambridge Crystallographic Data Centre, 12 Union Road, Cambridge CB2 1EZ, UK; fax: (+44) 1223–336–033; or e–mail: deposit@ccdc.cam.ac.uk.

Acknowledgments

This work was supported by National Natural Science Foundation of China (Grant 21371040 and 21171044), the National key Basic Research Program of China (973 Program, No. 2013CB632900), Fundamental Research Funds for the Central Universities (Grant No. HIT. IBRSEM. A. 201409), and Program for Innovation Research of Science in Harbin Institute of Technology (PIRS of HIT No. A201416 and B201414).

References

1 N. B. Shustova, A. F. Cozzolino, S. Reineke, M. Baldo, M. Dincaã, *J. Am. Chem. Soc*., 2013,**135,** 13326.

2 J. N. Hao, B. Yan, *J. Mater. Chem. C*, 2014, **2,** 6758.

3 Z. Zhang, W. X. Feng, P. Y. Su, X. Q. Lü, J. R. Song, D. D. Fan, W. K. Wong. R.

A. Jones, C. Y. Su, *Inorg. Chem*., 2014, **53,** 5950.

4 P. R. Matthes, J. Nitsch, A. Kuzmanski, C. Feldmann, A. Steffen, T. B. Marder, K. Müller-Buschbaum, *Chem. Eur. J*., 2013, **19,** 17369.

5 H. B. Zhang, L. J. Zhou, J. Wei, Z. H. Li, P. Lin, S. W. Du, *J. Mater. Chem*., 2012, **22,** 21210.

6 Z. Q. Xia, Q. Wei, Q. Yang, C. F. Qiao, S. P. Chen, G. Xie, G. C. Zhang, C. S. Zhou, S. L. Gao, *CrystEngComm*, 2013, **15,** 86.

7 S. Biju, M. L. P. Reddy, A. H. Cowley, K. V. Vasudevan, *Cryst. Growth Des*., 2009, **9,** 3562.

8 M. Hatanaka, K. Morokuma, *J. Chem. Theory Comput*., 2014, **10,** 4184.

9 R. Shyni. S. Biju, M. L. P. Reddy, A. H. Cowley, M. Findlater, *Inorg. Chem*., 2007, **46,** 11025.

10 J. Gregoliński, P. Starynowicz, K. T. Hua, J. L. Lunkley, G. Muller, J. Lisowski, *J. Am. Chem. Soc*., 2008, **130,** 17761.

11 C. W. Tang, S. A. VanSlyke, *Appl. Phys. Lett*., 1987, **51,** 913.

12 M. F. Wang, X. J. Hong, Q. G. Zhan, H. G. Jin, Y. T. Liu, Z. P. Zheng, S. H. Xu, Y. P. Cai, *Dalton Trans*., 2012, **41,** 11898.

13 G. Holger, K. Gerhard. *Angew. Chem. Int. Ed*., 2002, **41,** 48.

14 K. Müeller-Dethlefs, P. Hobza, *Chem. Rev.*, 2000,**100,** 143.

15 T. W. Duan, B. Yan, *J. Mater. Chem. C*, 2014, **2,** 5098.

16 L. D. Carlos, R. A. S. Ferreira, V. Z. Bermudez, B. Julián-López, P. Escribano, *Chem. Soc. Rev*., 2011, **40,** 536.

17 C. Sanchez, P. Belleville, M. Popall, L. Nicole, *Chem. Soc. Rev*., 2011, **40,** 696.

18 S. Rodríguez, P. Elizondo, S. Bernès, N. Pérez, R. Bustos, E. García-España, *Polyhedron*, 2015, **85,** 10.

19 C. B. Liu, Q. Li, X. Wang, G. B. Che, X. J. Zhang, *Inorg. Chem. Commun*., 2014, **39,** 56.

20 N. Wei, M. Y. Zhang, X. N. Zhang, G. M. Li, X. D. Zhang, Z. B. Han, *Cryst. Growth Des*., 2014, **14,** 3002.

21 T. J. Sørensen, L. R. Hill, J. A. Tilney, O. A. Blackburn, M. W. Jones, M.

Tropiano, S. Faulkner, *Eur. J. Inorg. Chem*., 2014, **15,** 2520.

22 K. Miyata, T. Nakanishi, K. Fushimi, Y. Hasegawa, *J. Photochem. Photobiol. A: Chem.*, 2012, **235**, 35.

23 C. X. Ding, X. Rui, C. Wang, Y. S. Xie, *CrystEngComm*, 2014, **16,** 1010.

24 X. P. Yang, D. Schipper, L. J. Zhang, K. Q. Yang, S. M. Huang, J. J. Jiang, C. Y. Su, R. A. Jones, *Nanoscale*, 2014, **6,** 10569.

25 A. Q. Zhang, J. L. Zhang, Q. L. Pan, S. H. Wang, H. S. Jia, B. S. Xu, *J. Lumin*., 2012, **132,** 965.

26 J. W. Dai, M. L. Tong, CrystEngComm, 2012, 14, 2124.

27 J. H. Liao, W. S. Hwang, G. Y. Chen, *Z. Anorg. Allg. Chem*., 2014, **640,** 1793.

28 K. M. Sureshan, R. G. Gonnable, *CrystEngComm*, 2013, **15,** 1676.

29 M. Zhu, Z. M. Hao, X. Z. Song, X. Meng, S. N. Zhao, S. Y. Song, H. J. Zhang, *Chem. Commun*., 2014, **50,** 1912.

30 G. L. Zhuang, X. J. Kong, L. S. Long, R. B. Huang, L. S. Zheng, *CrystEngComm*, 2010, **12,** 2691.

31 D. B. A. Raj, S. Biju, M. L. P. Reddy, *Inorg. Chem*., 2008, **27,** 8091.

32 Z. P. Zheng, Y. J. Qu, X. J. Hong, L. M. Wei, L. T. Wan, W. H. Zhou, Q. G. Zhan, Y. P. Cai, *Inorg. Chem*., 2014, **53,** 9625.

33 S. Chen, R. Q. Fan, S. Gao, X. M. Wang, Y. L. Yang, *J. Lumin*., 2014, **149,** 75.

34 J. D. Xu, T. M. Corneillie, E. G. Moore, G. L. Law, N. G. Butlin, K. N. Raymond. *J. Am. Chem. Soc*., 2011, **133,** 19900.

35 P. Wang, R. Q. Fan, Y. L. Yang, X. R. Liu, P. Xiao, X. Y. Li, W. L. J. Hasi, W. W. Cao, *CrystEngComm*, 2013, **15,** 4489.

36 B. Chu, W. L. Li, Z. R. Hong, F. X. Zang, H. Z. Wei. D. Y. Wang, M. T. Li, X. C. S. Lee, S. T. Lee, *J. Phys. D: Appl. Phys*., 2006, **39,** 4549.

37 S. Q. Su, W. Chen, C. Qin, S. Y. Song, Z. Y. Guo, G. H. Li, X. Z. Song, M. Zhu, S. Wang, Z. M. Hao, H. J. Zhang, *Cryst. Growth Des*., 2012, **12,** 1808.

38 D. B. Ambili Raj, B. Francis, M. L. P. Reddy, R. R. Butorac, V. M. Lynch, H. Cowley. *Inorg. Chem*., 2010, **49,** 9055.

39 R. Shyni, S. Biju, M. L. P. Reddy, A. H. Cowley, M. Findlater, *Inorg. Chem.*,

2007, **46,** 11025.

40 W. B. Sun, P. F. Yan, G. M. Li, H. Xu, J. W. Zhang, *J. Solid State Chem*., 2009, **182,** 381.

41 T. R. Wang, P. Li, H R. Li, *ACS Appl. Mater. Interfaces*, 2014, **6,** 12915.

42 P. Martín-Ramos, V. Lavín, M. R. Silva, I. R. Martín, F. Lahoz, P. Chamorro-Posada, J. A. Paixão, J. Martín-Gil, *J. Mater. Chem. C*, 2013, **1,** 5701.

43 S. Biju, Y. K. Eom, J. G. Bünzli, H. K. Kim, *J. Mater. Chem. C*, 2013, **1,** 6935

Table 1 Crystal data and structure refinements for complexes **1–9**

		1	**2**	**3**	**4**	**5**	**6**	**7**	**8**	**9**
Empirical formula		$C_{20}H_{26}N_2O_{11}ClEu$	$KC_{34}H_{27}ClN_5O_6Eu$	$C_{32}H_{22}N_5O_8Eu$	$C_{30}H_{28}N_3O_{11}Eu$	$C_{30}H_{28}N_3O_{11}Eu$	$C_{30}H_{28}N_3O_{11}Sm$	$C_{30}H_{28}N_3O_{11}Gd$	$C_{30}H_{28}N_3O_{11}Tb$	$C_{30}H_{28}N_3O_{11}Dy$	$C_{30}H_{28}N_3O_{11}Ho$
Formula weight		732.39	789.02	756.51	758.51	756.91	763.80	765.48	769.05	771.48
Crystal system		Monoclinic	Triclinic	Monoclinic	Triclinic	Triclinic	Triclinic	Triclinic	Triclinic	Triclinic
Space group		Pc	$P\bar{1}$	$P2_1/n$	$P\bar{1}$	$P\bar{1}$	$P\bar{1}$	$P\bar{1}$	$P\bar{1}$	$P\bar{1}$
a/Å		7.671(5)	11.1063(4)	14.8782(13)	7.842(5)	7.8460(16)	7.8374(16)	7.834(3)	7.8379(16)	7.821(3)
b/Å		6.820(5)	11.3995(5)	13.0813(9)	11.416(7)	11.390(2)	11.382 (2)	11.385(4)	11.390(2)	11.361(3)
c/Å		25.658(18)	14.9133(6)	17.2576(14)	16.613(10)	16.620(3)	16.602(3)	16.574(6)	16.582(3)	16.558(5)
α (°)		90	111.9660(10)	90	81.716(7)	81.81(3)	81.96(3)	81.799(4)	81.94(3)	81.889(4)
β (°)		94.011(10)	91.3200(10)	110.253(2)	87.825(7)	87.79(3)	87.88(3)	87.851(4)	87.87(3)	88.034(12)
γ (°)		90	111.1270(10)	90	79.381(7)	79.34(3)	79.49(3)	79.435(4)	79.35(3)	79.629(3)
Volume/Å^3		1339.2(16)	1605.93(11)	3151.1(4)	1446.5(15)	1444.6(5)	1441.7(5)	1438.2(9)	1440.4(5)	1432.7(8)
Z		2	2	4	2	2	2	2	2	2
D_{calcd}/Mg·m^{-3}		1.186	1.632	1.595	1.742	1.740	1.759	1.768	1.773	1.788
μ/mm^{-1}		2.755	2.090	2.049	2.237	2.101	2.369	2.528	2.663	2.831
F(000)		728	788	1504	760	758	762	764	766	768
θ range (°)		1.59–24.84	3.00–25.76	3.11–25.40	1.83–25.02	3.07–27.48	3.08–27.47	1.24–26.95	3.07–27.48	1.24–26.90
Limiting indices		$-9 \le h \le 9$ $0 \le k \le 8$ $0 \le l \le 30$	$-13 \le h \le 13$ $-11 \le k \le 13$ $-18 \le l \le 18$	$-17 \le h \le 17$ $-15 \le k \le 14$ $-20 \le l \le 20$	$-9 \le h \le 9$ $-13 \le k \le 13$ $-19 \le l \le 19$	$-10 \le h \le 9$ $-14 \le k \le 14$ $-21 \le l \le 21$	$-10 \le h \le 9$ $-14 \le k \le 14$ $-21 \le l \le 21$	$-9 \le h \le 9$ $-14 \le k \le 13$ $-19 \le l \le 21$	$-10 \le h \le 8$ $-14 \le k \le 14$ $-21 \le l \le 21$	$-9 \le h \le 9$ $-14 \le k \le 13$ $-20 \le l \le 19$
GOF on F^2		1.089	1.072	1.042	1.192	1.074	1.095	1.214	1.092	1.165
Final R indices	R_1 [a]	0.0883	0.0282	0.0547	0.0586	0.0353	0.0297	0.1029	0.0361	0.0401
[$I > 2\sigma(I)$]	wR_2 [b]	0.1973	0.0657	0.1378	0.1645	0.0838	0.1001	0.2206	0.0920	0.1166
R indices	R_1	0.1181	0.0363	0.1072	0.0640	0.0449	0.0331	0.1074	0.0439	0.0500
(all data)	wR_2	0.2189	0.0757	0.1690	0.1667	0.0875	0.1075	0.2228	0.0960	0.1257

[a] $R_1 = \sum||F_o| - |F_c||/\sum|F_o|$. [b] $wR_2 = \{\sum[w\,(F_o^2 - F_c^2)^2]/\sum[\,w\,(F_o^2)^2]\}^{1/2}$.

Structure variations of series lanthanide complexes constructed from quinoline carboxylate ligand: photoluminescent properties and PMMA matrices doping

Huijie Zhang,[a] Ruiqing Fan,*,[a] Ping Wang,[a] Xinming Wang,[a] Song Gao, [a] Yuwei Dong,[a] Yulei Wang, [b] Yulin Yang*,[a]

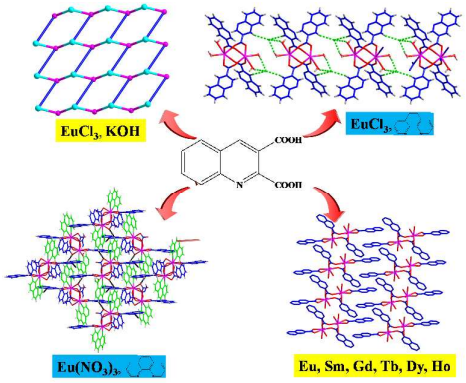

Series of lanthanide complexes constructed by H_2qldc have been synthesized and the luminescence properties have been discussed.